Numerical simulation of mechanical resistance of wet and dry powder cakes

Zahra Afrassiabian, Willy Leclerc, Mohammed Guessasma, Khashayar Saleh

▶ **To cite this version:**

Zahra Afrassiabian, Willy Leclerc, Mohammed Guessasma, Khashayar Saleh. Numerical simulation of mechanical resistance of wet and dry powder cakes. Powder Technology, 2020, 371, pp.45 - 54. ⟨10.1016/j.powtec.2020.05.040⟩. ⟨hal-03490782⟩

HAL Id: hal-03490782

https://hal.science/hal-03490782v1

Submitted on 6 Jun 2022

HAL is a multi-disciplinary open access archive for the deposit and dissemination of scientific research documents, whether they are published or not. The documents may come from teaching and research institutions in France or abroad, or from public or private research centers.

L'archive ouverte pluridisciplinaire **HAL**, est destinée au dépôt et à la diffusion de documents scientifiques de niveau recherche, publiés ou non, émanant des établissements d'enseignement et de recherche français ou étrangers, des laboratoires publics ou privés.

Distributed under a Creative Commons CC BY-NC 4.0 - Attribution - Non-commercial use - International License

Version of Record: https://www.sciencedirect.com/science/article/pii/S0032591020304034
Manuscript_8a00f972afff59c09d5918996704e849

Numerical simulation of mechanical resistance of wet and dry powder cakes

Zahra Afrassiabian[1], Willy Leclerc[2], Mohammed Guessasma[2], Khashayar Saleh[1]

[1] TIMR EA-4297, Université de Technologie de Compiègne, Sorbonne Universités, 60200 Compiègne, France

[2] Laboratoire des Technologies Innovantes, EA 3899, UPJV, 02100, Saint Quentin, France

khashayar.saleh@utc.fr

Abstract

This paper presents a multi-scale modelling approach to describe the mechanical behaviour of caked powders as an aid to properly design and analyse the results of laboratory caking tests to assess the propensity of powders to cake. This approach is based on the integration of particle-particle interactions due to liquid or solid bridges over the total volume of a cake using Discrete Element Method (DEM). The overall objective of the study was to simulate the behaviour of agglomerated (caked) samples subjected to a mechanical, compressive or tractive, stress. First, simulations were performed on an assembly of particles subjected to capillary forces. The capillary forces being amenable to a theoretical description, the tensile strength of wet agglomerates was calculated theoretically and used as a reference to validate the numerical results. Simulations were based on the combination of conventional DEM method and the phenomenological model of capillary condensation. The stress-strain curves were then simulated and compared to the theoretical values predicted by Rumpf's model for wet agglomerates. After validation, numerical simulations were used to study the mechanical behaviour of wet or dry agglomerates subjected to compression. In order to take into account the cohesive effect of solid bridges at the level of elementary contacts in discrete modelling, an original Euler-Bernoulli type beam model between particles in contact was established. The simulated stress-strain results was in very good agreement with experimental data.

Keywords: DEM simulation, yield stress, caking, agglomeration, capillary condensation, solid bridges, beam model.

© 2020 published by Elsevier. This manuscript is made available under the CC BY NC user license
https://creativecommons.org/licenses/by-nc/4.0/

1 Introduction

Powdered products are a significant part of finished or intermediate products encountered in the various industrial sectors [1]. However, despite the numerous benefits of powders, their handling and storage often cause some severe problems (*i.e.*, explosion, clogging, dust generation, *etc.*). This could lead to a destruction of products and even their corresponding manufacturing units or to deterioration of the expected functionalities of products. Among these issues, caking of powders is undoubtedly one of the most detrimental phenomena in terms of their end-use properties. Generally speaking, caking corresponds to spontaneous and undesired formation of a coherent mass from individual grains [2]. Caking phenomenon occurs as a result of formation of material bonds at the contact points between particles. These links, whose fundamental mechanisms of appearance are still insufficiently understood, are reinforced by pressure, the migration of matter and variations in humidity and temperature. Note also that this unwanted agglomeration of particles of a powder is often very slow, irreversible and difficult to predict. In this context, it is essential to have predictive tools (caking tests or numerical models) to characterize, as reliably as possible, the propensity of the powders to cake in a given environment.

A multitude of methods has been reported in the literature to characterize the propensity of powders to cake [3, 4]. The test methods reported in the literature range from very basic tests (drop test) to much more sophisticated tests such as shear tests.

The common point of all these methods is that they include two stages [5, 6]:

- The first step consists in placing the powder under conditions such that bonds will form between the particles. This can be done by applying a stress (formation of van der Waals bonds or solid bonds), by humidifying the powder (liquid bridges) or by subjecting the powder to a moisture and/or temperature cycle (formation of solid bridges)
- Once the powder has been caked, the sample can then be characterized mechanically by methods such as shear, compression, traction or indentation tests.

One of the main challenges in the characterization of caking remains the determination of the mechanical strength of the cake. Zafar *et al.* [3] and Carpin *et al.* [4] reviewed the different tests reported in the literature. These authors made a classification of tests based on the

method used to measure the mechanical resistance of cakes. They distinguish mechanical test methods including shear cell, uniaxial compression, tensile, ICI, penetration and powder rheometer testings as well as alternative tests (sensory, sieving, sticky point measurement, blow tester, microscopic observations, *etc.*). Because the caking is a slow process, the preparation of cakes is generally accelerated by prior wetting of powders or by using an air current instead of stagnant air. Moreover, in a recent work, [7] Samain provided an extensive review of the caking tests by crossing the methods to prepare the caked samples and those used to characterize the cakes. These works clearly showed that, the existing tests suffer from a poor repeatability, a part of which is often inherent in the system, but also because of inadequate testing methods or non-optimized cake geometry. On the other hand, there is still no reliable theoretical model to describe the dynamic behavior of a powder bed during mechanical tests under compression, traction or shear. The most used model in this field is that of Rumpf but this model corresponds to the tensile strength of a static stack of grains when in practice, it is practically impossible to perform the tensile tests (but compression or shearing) and in addition, tests are dynamic rather than static. There is therefore a need to establish new models in order to better describe the behavior of cakes during different solicitations and to be able to simulate this behavior. This allows the experiments to be well designed and the data to be better interpreted for a more reliable assessment of caking behavior. This is crucial for a better understanding of the phenomena and decoupling them to extract the intrinsic properties of the cakes. However, modelling of dispersed media in order to link microscopic phenomena occurring at the particle scale to their overall macroscopic behaviour remains still a major challenge in powder science and technology. In the case of wet agglomeration or caking, for example, given the complexity of phenomena occurring simultaneously at particle's scale (*i.e.*, adsorption, absorption, capillary condensation, crystallization, diffusion, desorption, liquid or solid bridging, etc.) on the one hand, and the heterogeneity of the system (shape, size, composition, etc.), on the other hand, a detailed description of the media, even on a small scale, remains almost inaccessible. To this must be added the problem of the excessive number of particles present in real systems, which makes a complete description of the system almost impossible until now.

In the present work, a method based on DEM simulation of granular media based on use of multiple modelling approaches across length scales is developed to describe the mechanical

resistance of wet or dry agglomerated (caked) samples. use of. The purpose of simulations was to provide a better understanding and interpretation of the experimental results taking into account the phenomena related to the heterogeneity of the medium as well as to have a reliable numerical tool for the prediction of the behaviour of cakes in the conditions other than those experimentally tested.

From a numerical cost point of view, both CPU time and memory depend strongly on the density of the simulated granular packing. Regarding the numerical simulations carried out in this study, the maximum number of particles that composed the agglomerated powder is in the order of 10,000 which does not lead a large computational time. Typically, one day in length for one simulation.

Firstly, the simulations were carried out on the tensile strength of wet cakes due to the presence of liquid bridges. The results for tensile strength of wet cakes calculated by a phenomenological model were used as a reference case to validate the consistency of simulation results. After validation, DEM simulations were used to describe the yield stress of cakes resulting from different attractive forces (liquid bridge, solid bridge, *etc.*). The validation of the model was carried out based on the experimental data of the authors published elsewhere [5, 6].

1.1 Brief reminder of previous works

1.1.1 Experimental data

Experimental data used in this study regarding the procedure of cake preparation and the post-caking tests in order to validate the model have already been published elsewhere [5, 6] and will not be detailed here. Very briefly, the caking experiments were conducted in a multi-cell caking device allowing to prepare cylindrical compacts (40mm ID, 26 mm height) under accelerated (humid air crossing the samples) and controlled conditions (T, RH, P, air flow rate). The mechanical resistance of cakes was then measured using different tests: uniaxial compression, diametral compression (Brazilian test) as well as shearing (translational) test.

1.1.2 Modelling

In a previous work, Afrassiabian *et al.* [2] established a phenomenological model of capillary condensation in granular media under humid conditions. This approach is based on the integration of water condensation and liquid bridge formation within binary contacts in regular or random packing of particles. The model was based on the combination of Kelvin law of capillary condensation and Laplace law for capillary forces. Briefly, the model predicts first the water activity, a_w corresponding to a liquid bridge formed between two spherical particles with radii R (Figure 1). Knowing the filling angle, ψ, and the interparticle gap, h, the geometry (principal radii of curvature, ϱ_1 and ϱ_2 and consequently the volume, V_L) of the liquid bridge can be obtained by the following set of equations:

$$\varrho_1 = \frac{-R(1 - cos\,\psi) + h}{cos(\psi + h)} \tag{1}$$

$$\varrho_2 = R\,sin\,\psi - \varrho_1\,[1 - sin(\psi + h)\,] \tag{2}$$

$$V_L = \int_{x_1}^{x_2} \pi \left(\varrho_1 + \varrho_2 - \sqrt{\varrho_1^2 - x^2} \right)^2 dx \; - \frac{2\pi R^3}{3}\,(2 - 3\,cos\,\psi - \cos^3\psi) \tag{3}$$

All symbols are illustrated in Figure 1.

Knowing ϱ_1 and ϱ_2, the equivalent capillary (Kelvin) radius and the corresponding water activity can be calculated as follow:

$$\frac{1}{r_c} = \frac{1}{2}\left(\frac{1}{\varrho_1} + \frac{1}{\varrho_2}\right) \tag{4}$$

$$\ln a_w = \frac{-2\,\upsilon_L \cdot \gamma}{r_c \cdot \mathcal{R} \cdot T} \tag{5}$$

where γ is the vapor–liquid surface tension, $\mathcal{R}$ the universal gas constant, T the temperature, and υ_L the molar volume of liquid.

Furthermore, according to Laplace theory for capillary forces, the total attractive force between the two particles including both the capillary and the surface tension components is given by [8]:

$$F_{cap} = 4\pi R\gamma \sin(\psi)\left[\sin(\psi + \theta) + \frac{R}{2}\sin\psi\left(\frac{1}{\varrho_1} + \frac{1}{\varrho_2}\right)\right] \tag{6}$$

Finally, the tensile strength of a random packing of monosize particles can be estimated by Rumpf's model:

$$\sigma_T = \frac{1-\varphi}{\pi}\frac{Z}{d_p^2}\cdot F \tag{7}$$

where ε is the mean void fraction of the bed, k is the average coordination number of the packing and F is the average force between two single particles. In the case of liquid bridges $F = F_{cap}$.

2 DEM simulation of mechanical strength of agglomerates

2.1 Basic concepts and equations

Discrete numerical modelling was first used to study the effect of capillary condensation in granular media at a Representative Element of Volume (REV). This amounts to solving the classical equations of dynamics for a particle assembly. This method has already been used to model the behaviour of granular materials in the presence of capillary forces [9, 10]. The advantage of a discrete approach lies particularly in its ability to integrate physical quantities by being closer to the microstructure of the granular medium (at contact scale). Expressed in the global coordinate system, the set of equations originally developed by Cundall and Strack [11-13] is the following:

$$\begin{cases} m_i\ddot{u} = F_i^{ext} + \sum_j F^{j\to i} \\ I_i\ddot{\theta} = M_i^{ext} + \sum_j M^{j\to i} \end{cases} \tag{8}$$

where $\ddot{u}$ and $\ddot{\theta}$ are linear and angular acceleration vectors, respectively, m_i and I_i are the mass and the moment of inertia matrix of the particle i, $F^{j\to i}$ and $M^{j\to i}$ the force and moment vectors due to the action of the particle j on the particle i, and F_i^{ext} and M_i^{ext} the external force and moment vectors.

Mechanical contact interactions are calculated with an explicit contact law [11]. The particles were assimilated to rigid spheres. The contact forces in the absence of capillary effect were presented with a linear contact model depending on elastic force displacement law, Coulomb friction and viscous damping coefficient. For a pair of particles in contact $(i;\ j)$ the

normal and tangential forces, $F_{n,t}$, expressed in the coordinate system related to the contact plane were provided by the Kelvin-Voigt model:

$$\begin{cases} F_{n,t} = -k_{n,t}\,\delta_{n,t} - c_{n,t}\,v_{n,t} \\ with:\ F_t = -min(|F_t|, \mu|F_n|) \times sign(v_t) \\ \dfrac{k_t}{k_n} \in \left[\dfrac{2}{3}, 1\right] \\ c_{n,t} = 2\sqrt{k_{n,t} m^*} \end{cases} \quad (9)$$

where $k_{n,t}$ and $c_{n,t}$ are the normal and tangential stiffness of contact and damping coefficients, respectively, and μ is the dry friction coefficient of Coulomb. $\delta_{n,t}$ and $v_{n,t}$ are the relative displacements and velocities, respectively, according to the normal and tangential directions. The repulsive force, *i.e.*, normal force, is obtained according to Hertz theory where the normal stiffness k_n is function of the elastic moduli and the effective radius of both particles in contact [11]. The normal stiffness k_n $\left(k_n = 2\,E_{ff}\sqrt{R_{eff}\delta_n}\right)$ is proportional to $\delta_n^{1/2}$ inducing a nonlinear normal force $\left(F_n \propto \delta_n^{3/2}\right)$, where E_{eff} $\left(\frac{1}{E_{eff}} = \frac{1-\nu_i^2}{E_i} + \frac{1-\nu_j^2}{E_j}\right)$ is the effective modulus of elasticity function of Young's moduli, E_i and E_j and the Poisson's ratios, ν_i and ν_i, of the two contacting particles. R_{eff} is the effective radius $\left(R_{eff} = \frac{R_i R_j}{R_i + R_j}\right)$, with R_i and R_j the radii of particles in contact i and j, respectively. The tangential force is calculated by means of the tangential stiffness k_t $\left(\,k_t = 8\,G_{eff}\sqrt{R_{eff}\delta_n}\right)$, where G_{eff} is the effective shear modulus.

The mechanical system requires an explicit time integration based on the velocity-Verlet scheme:

$$\begin{cases} u(t+\Delta t) = u(t) + \Delta t\,\dot{u}(t) + \dfrac{\Delta t^2}{2}\ddot{u}(t) \\ \dot{u}(t+\Delta t) = \dot{u}(t) + \dfrac{\Delta t}{2}(\ddot{u}(t) + \ddot{u}(t+\Delta t) \end{cases} \quad (10)$$

DEM simulations were carried out using the MULTICOR-3D and MULTICOR3D++ discrete element codes [14, 15]. The method allows describing both the case of liquid capillary and solid bridges.

2.1.1 Discrete simulation of liquid bridges

In the presence of capillary bridges, the normal component of the contact force F_n is the resultant of repulsive and attractive interactions:

$$F_n = -k_n\delta_n - c_n v_n - F_{cap} \quad (11)$$

The attractive interaction, F_{cap} , due to the capillary effect is obtained according to Rumph's model [8] taking into account the filling angle, ψ, and the principal radii of curvature ϱ_1 and ϱ_2. More specifically, at each pair of particles with interparticle gap $2h$, the filling angle is calculated iteratively using the Newton-Raphson algorithm with less than 50 iterations and an accuracy of 10^{-6} rad. Indeed, since the number of capillary bridges may change during the simulation, this leads to run the contact detection algorithm at each time step. This of course means that the filling angle for each contact has also to be updated appropriately. Nevertheless, the numerical cost of the capillary bridge updating can be considered as minor in comparison to the contact detection cost. By running the Newton-Raphson algorithm, the filling angle is obtained with less than 50 iterations and an accuracy of $10^{-6}\ rad$. Moreover, as well-known, the contact detection process is by far the costliest step in discrete element method. Once the filling angle is calculated, the principal radii of curvature are determined and the attractive force is then calculated. It should be pointed out that h and δ_n are the same and both express the difference between the centre to centre distance separating two particles and $2R$ (Figure 1).

In this study, it is assumed that the tangential effect of the capillary bridge is negligible and that, in addition, the wettability is perfect (contact angle $\theta = 0$). The viscous effect of liquid was also neglected in the modelling because the main liquid involved in caking is water, which is not very viscous. The capillary force at each contact point was then calculated using Eq. (6).

2.1.2 Discrete simulation of solid bridges (Beam model)

This section deals with the mechanical behaviour of powders containing solid bridges. In order to take into account the cohesive effect of solid bridges at the level of elementary contacts in discrete modelling, we have introduced an Euler-Bernoulli type beam model between particles in contact. This approach has been developed by LTI/UPJV and have been described in details elsewhere [16-18].

In this model, the solid bridges are assimilated to beams linking the particles together. The local (or microscopic) parameters that characterize the beam model are E_μ, G_μ, A_μ and L_μ, respectively the Young's modulus, the shear (or Coulomb) modulus, the cross-section of the beam and the length of the beam (Figure 2). In a matrix form, the generalized forces of cohesion induced by the beam are calculated via a matrix of stiffness (Eq. 12) [19]. At the end of each beam element $(i;\ j)$ are affected the degrees of freedom in translation, $u_n^{i,j}$, $u_t^{i,j}$, $u_f^{i,j}$, and in rotation $\theta_n^{i,j}$, $\theta_t^{i,j}$, $\theta_f^{i,j}$, expressed in the local base of the beam ($\vec{u}_n$, $\vec{u}_t$, $\vec{u}_f$). The subscripts n, t and f are related to the normal, tangential and bending effects, respectively.

The cohesion forces between two particles, i and j, are represented by the following system:

$$\begin{bmatrix} F_n^{j\to i} \\ F_t^{j\to i} \\ F_f^{j\to i} \\ M_n^{j\to i} \\ M_t^{j\to i} \\ M_f^{j\to i} \end{bmatrix} = \begin{bmatrix} K_n & 0 & 0 & 0 & 0 & 0 & 0 & 0 \\ 0 & K_t & 0 & 0 & 0 & 0 & \frac{K_t L_\mu}{2} & \frac{K_t L_\mu}{2} \\ 0 & 0 & K_t & 0 & -\frac{K_t L_\mu}{2} & -\frac{K_t L_\mu}{2} & 0 & 0 \\ 0 & 0 & 0 & S_n & 0 & 0 & 0 & 0 \\ 0 & 0 & -\frac{K_t L_\mu}{2} & 0 & \frac{K_t L_\mu^2}{3} & \frac{K_t L_\mu^2}{6} & 0 & 0 \\ 0 & \frac{K_t L_\mu}{2} & 0 & 0 & 0 & 0 & \frac{K_t L_\mu^2}{3} & \frac{K_t L_\mu^2}{6} \end{bmatrix} \begin{bmatrix} u_n^i - u_n^j \\ u_t^i - u_t^j \\ u_f^i - u_f^j \\ \theta_n^i - \theta_n^j \\ \theta_t^i \\ \theta_t^j \\ \theta_f^i \\ \theta_f^j \end{bmatrix} \quad (12)$$

where $F_n^{j\to i}$, $F_t^{j\to i}$, $F_f^{j\to i}$, $M_n^{j\to i}$, $M_t^{j\to i}$ and $M_f^{j\to i}$ are the components of the vector of generalized forces of cohesion expressed in the local base of the beam and k_n, k_t and S_n of the matrix are the local stiffnesses, with: $K_n = \frac{E_\mu A_\mu}{L_\mu}$, $K_t = \frac{12 E_\mu I}{L_\mu^3}$ and $S_n = \frac{2 G_\mu I_\mu}{L_\mu}$. I_μ is the

quadratic moment. Note that the radius a_μ of the cross section A_μ of the beam depends on a dimensionless parameter, r_μ, such that: $a_\mu = r_\mu \frac{R_i+R_j}{2}$. The behaviour of the beam is therefore a function of the local Young's modulus E_μ and the dimensionless parameter, $r_\mu \in$]0,1].

3 Results and discussion

3.1 Discrete simulations of capillary effects at a REV scale

First, we focus on the role of capillary condensation and subsequent liquid bridge formation within a granular medium exposed to fluctuations of ambient relative humidity. As we saw in the previous section, such bridges cause an attractive force between particles, leading to the formation of a cake with intrinsic physicochemical and mechanical properties. By considering a Representative Elementary Volume (REV) of 10.000 particles, the DEM was then performed by means of MULTICOR3D software taking into account the properties of the cake (degree of saturation) in order to establish relationships between the microscopic parameters and the macroscopic behavior (tensile strength) of cakes. The software uses the explicit (also called smoothed) formulation [20] which enables to fulfil the assumptions of the Random Close Packing (RCP).

DEM simulations were based on the combination of conventional DEM method and the phenomenological model of capillary condensation, presented in the previous section. At each step of time, capillary forces at each binary contact were calculated by assuming that the system is in thermodynamic equilibrium (a_w=RH). The volume of liquid bridges and the extent of capillary forces within a known arrangement of particles at a desired water activity was calculated by the combination of the Kelvin law of capillary condensation and the Laplace law for capillary forces, as explained earlier:

- Initially, the degree of saturation in water was set at a given value, the corresponding volume of liquid was distributed equitably over the potential contacts ($0 < 2h^* < 0.3$), with $h^* = \frac{h}{R}$.
- At each time step, the geometric parameters of each capillary bridge $(\psi, \varrho_1, \varrho_2)$ were obtained by an iterative calculation.

- Finally, the redistribution of the liquid volume for the following time step was calculated based on the evolution of the contacts.

Figure 3 presents a snapshot from MULTICOR3D software, showing four binary contacts for different dimensionless separating distances ($2h^* = 0.02;\ 0.08;\ 0.20;\ 0.30$). At each contact, the capillary bridge shape is drawn with respect to their respective geometric parameters, namely the principal radii, $\varrho_1,\ \varrho_2$ and the filling angle, ψ.

3.2 Densification of regular packings under the effect of capillary bridges

Initially, the implementation of DEM allowed to model the effect of capillary condensation on regular packing of particles (CS, CC and CFC), with a particle radius of R=1.5 µm. The objective was to simulate the densification of stacks initially generated with non-contact particles ($0 < 2h^* < 0.3$). After having fixed the degree of saturation, the creation of capillary bridges between particles mechanically leads to a densification of the stack. At the end of this step, the theoretical values of compactness are verified respectively for the different studied cases, namely 52% for the CS, 68% for the CC and 74% for the CFC packing (Figure 4-a). The results of Figure (4-b) show a homogeneous densification of the stack. The kinetics of densification of all the particles was similar to the behaviour of two isolated particles. These test cases are, of course, not representative of the actual packings, but they allow to be placed in an ideal case without rearrangement and thus to validate the results provided by the discrete model.

3.3 Mechanical behaviour of powder compacts in the presence of capillary bridges

In a second time, the DEM was used to characterize the behaviour of an assembly of monodisperse particles in order to study the influence of the particle size and the degree of saturation on randomly generated packing of particles. The characteristics of the powder compacts and the tensile test parameters are summarized in table 1. The granular packing was generated by the efficient Lubachevsky-Stillinger Algorithm (LSA) [20]. Considering a constant

box volume, $(10^{-4})^3\ m^3$, six packings are generated with a number of particles varying in the interval $[2 \times 10^3; 2 \times 10^4]$, a particle radius ranging between 2 µm and 4 µm, a constant compactness (≈50%) and a density of 1500 kg.m^3. The degree of saturation, S, varies within the interval [0.64%; 12.8%].

The numerical characterization of the behaviour was carried out through a simple tensile test with an imposed speed of 10^{-4} m.s^{-1} and a time step of 10^{-7} s. The six stacks were submitted to simple tension in order to highlight a possible influence of their behaviour as a function of particle size. It should be reminded here that the initial volume of the domain is constant regardless of the number of particles in the stack. At the beginning, when the capillary links at the contacts are created, the packing is in a state of agitation (Figure 5-a). Therefore, before applying the tensile stress, a stabilization phase is necessary in order to reach the equilibrium state. Figure (5-a) provides information about the densification process of the stack with a kinetic energy close to zero when the equilibrium state is reached. Figure (5-b) and (c) present the capillary bridges and displacement field, respectively, at the end of the densification process. Once equilibrium state is achieved, the packing is subjected to a quasi-static tensile stress. During the test, the tensile stress, σ (Pa), is evaluated in the middle section of the packing to avoid edge effects, and the strain, ε (%), is estimated with respect to the particle radius.

The curves plotted in Figure 6 show the variation of the time-weighted tensile stress as a function of the relative elongation of the packing with a water saturation rate of 10.4%. The first observation concerns the two phases that characterize the first moments of the tensile test. Indeed, the traction curve has a very steep first phase, which reflects the reaction of the stack to the load. This sharp increase is followed very quickly by a second phase of low stiffness.

The second observation is related to the relative sensitivity of the maximum stress to particle size, even though the tensile curve is less and less erratic as the number of particles increases. Finally, the stack containing 20.000 particles is the one whose tensile curve shows a decrease in the slowest stress. This behaviour is partly explained by a high density of capillary links in the right section of the stack. This results in a wider flow area beyond the maximum stress.

Figure 6-b shows the evolution of a stack of 8000 particles at different times of the numerical tensile test. The wall placed at the middle of the stack allows computing with a good accuracy the tensile stress during the simulation in order to avoid a possible disturbance near the upper and lower boundaries. We note that there is no interaction at all between the particles and the middle wall as shown in figure 6-b. To avoid the boundary effects, a fictitious wall is considered, the role of which is only to localize those particles at the middle of the sample that are subjected to the tensile force.

The second study focused on the influence of the water saturation rate on the tensile strength. The number of particles was 10.000, which is a good compromise between accuracy and calculation time. The reference saturation rate was S = 0.64%. The test protocol is identical to that described above. Figure 7 shows a clear influence of the saturation rate on the tensile strength of the stack. The results show the evolution of the coordination number Z (mean number of capillary bridges by particle). This result was obviously expected, since a greater quantity of water increases both the intensity and the number of bridges. Indeed, this results in a coordination number, Z, which increases as a function of the saturation rate (Figure 7-b). This evolution is in agreement with the results of tensile tests. Moreover, during the upward phase of the test, the parameter Z decreases until the tensile force reaches its maximum. In fact, during this phase, the particles may lose capillary bridges because of the increasing of the gap between some particles and its neighbours $(2h^* > 0.3)$. Conversely, in the second phase of the test, when the sample is broken, the particles are no longer subjected to the tensile force, thereby facilitating the reactivation of new capillary bridges, thus increasing slightly the coordination number Z.

3.4 Mechanical behaviour of powder compacts in the presence of solid bridges

3.4.1 Calibration of beam properties and stress state at particle scale

The identification of the local properties of the beam, namely its normal and transverse rigidities (E_μ; G_μ) are obtained by means of a calibration technique, which makes it possible to link the macroscopic properties of a powder compact to the local parameters of the strong

interparticle links. Thus, it is possible from numerically obtained abacuses to identify the microscopic properties of the beam element in order to reproduce the behavior of a caked powder whose macroscopic properties have been experimentally characterized [15, 18]. At the end of the calibration process, local properties are thus assigned to the solid bonds of a caked powder, in order to reproduce numerically the desired macroscopic behavior. Mechanical tests of indirect tensile (Brazilian test) and shear tests were carried out using the MULTICOR3D++ discrete element simulation tool [15] on compacts of anhydrous lactose powder. The experimental characterization tests are detailed elsewhere [6].

The damage occurred during the mechanical tests in the specimen is taken into account by means of an appropriate failure criterion depending on the stress state in the particle. The cohesive links of a given particle fail when the material strength is reached. Two criteria are considered for the simulated mechanical tests. For Brazilian and shear tests, we have considered criteria based on hydrostatic stress and Mohr Coulomb model, respectively. In the case of discrete material, the virial stress does not characterize the measure for mechanical force between material points and cannot be considered as a measure for mechanical stress. Hence, we determine the stress state at the particle scale by using an equivalent Cauchy stress tensor $\bar{\sigma}_p^i$. This tensor was proposed by Zhou [21] for molecular dynamic simulations, and was used in DEM lately by Jebahi *et al.*[22]. The stress tensor is given by the following equation:

$$\bar{\sigma}_p^i = \frac{1}{2V_i} \sum_{j \in Z_i} \frac{1}{2} \left(d_{ij} \otimes f_{ij} + f_{ij} \otimes d_{ij} \right) \tag{13}$$

with V_i the volume of the particle i, Z_i the coordination number of the particle i, d_{ij} the position vector connecting the center of the particles i and j and f_{ij} the cohesive force vector acting on the particles i and j.

The mechanical tests were conducted on samples of cylindrical shape, of diameter D=40 mm, thickness $e = 16\,mm$ and mean void fraction $= 0.64$. The simulated compacts consist of 10^4 particles, with a mean diameter of d_m=675 µm. The indirect tensile and shear tests are controlled at a speed of amplitude of 1 mm.min^{-1}. The sample sizes and the test conditions were then identical to those imposed during the experimental campaign. The characteristics of the caked powder and the Brazilian and shear test parameters are summarized in table 2.

3.4.2 Brazilian test

Before performing numerically the brazilian test, we have adjusted E_μ, for a given, r_μ $(r_\mu \approx 0.72)$ to calibrate the macroscopic mechanical behavior of the caked powder, in terms of macroscopic Young's modulus, E_M and Poisson ratio, ν_M. The solid bridges at particle scale fail when the positive hydrostatic stress exceeds the uniaxial tensile strength of the material [15]. However, the value of the tensile strength of the particle should be first adjusted so that the simulated macroscopic strength is close to that obtained experimentally. Figure 8-a compares the numerical and experimental curves obtained in a Brazilian test. The mechanical response of the compact powder follows fairly well the experimental curve. In addition, the ultimate load reached by the sample is substantially close to that obtained during the experimental test. Also, Figure 8-b shows clearly a concentration of the tensile stress in the central zone of the sample. This type of mechanical test makes it possible to characterize the tensile strength of brittle materials. Finally, Figure 8-c qualitatively shows the presence of particles (particles coloured blue) whose interparticle bonds are broken.

This first trial demonstrated the ability of the simulation tools developed to reproduce the mechanical behaviour of a cohesive multicontact system. The quality of the results obtained is, however, conditioned by the calibration step discussed previously, hence the importance of a rigorous identification of the mechanical and geometric parameters of the solid bridges. Taking into account the breaking of solid bridges, using a rupture criterion based on the hydrostatic stress measured at the particle scale [18], it was possible to simulate and follow the state of mechanical degradation of the sample at the particle scale.

3.4.3 Shear test

The second type of simulated behavior was that obtained during a shear test on a cylindrical compact as explained in [23]. The diameter of the sample is identical to that considered in the case of indirect traction. The particle size of the caked powder also remains unchanged, namely an average diameter of the order of 675 microns. The shear test was simulated with a speed of 1 mm.mn^{-1} during the mechanical test. In the case of shear test, the solid bridges created between particles fail when the Mohr Coulomb criterion is not fulfilled.

Here we just recall that the Mohr Coulomb criterion is expressed by means of a combination of shear and normal stresses, depending on the minor and major principal stresses. In order to obtain a good agreement between the numerical curve and the experimental one, during the upward phase of the shear test, the shear strength at the particle scale should first be adjusted so that the simulated macroscopic strength is close to that obtained experimentally. Moreover, when the failure mechanism starts in the shear plane, the damaged particles are removed as well as the cohesive links between damaged particles and their neighbours, as proposed in Jebahi et al. [22] and Leclerc et al. [15, 18]. It should be noted that the failure criterion (Mohr-Coulomb criterion) depends on the stress field in the particle determined by means of the tensor formula suggested by Zhou [21].

The results are shown in Figure 9. It appears that the shear behaviour obtained numerically partially reproduces that observed experimentally (Figure 9-a). Indeed, the simulated load stage is substantially close to the experimental results. Nevertheless, when the resistance capacity of the compact decreases, the behaviour of the compact obtained by simulation differs significantly from that recorded during the experimental test. This difference can be caused by several factors, such as the boundary conditions, the criteria of rupture chosen or the number of particles in the sample. The implementation of other numerical simulations would make it possible to discriminate the most influencing parameters. Further investigation is required to improve this promising method. Also, a qualitative representation of the breaking of solid bridges is given in Figure 9-b. One can clearly distinguish the emergence of a shear plane between the upper and lower parts of the sample sliding by one another. This can in fact induces new contacts between particles of both sides of the shear plane, which consequently requires to run the contact detection algorithm at each time step. Furthermore, the emergence of new contacts in the shear plane is largely the cause of erratic decrease of the shear strength observed in figure 9-a. As both upper and lower parts of the sample slides over each other, this involves typically a stick-slip phenomenon, which is often observed for the contact interface issues.

4 Conclusion

In this work, we presented the results of a study on modelling and numerical simulation of mechanical resistance of caked samples. The numerical simulations were carried out based

on Discrete Element Method (DEM). The global objective of the study was to simulate the behaviour of the agglomerated (caked) samples subjected to a mechanical, compressive or shear, stress.

First, a phenomenological model was established based on a combination of the fundamental Kelvin and Laplace laws and Rumpf model for granular media. This model allows to describe theoretically the relationships between the water activity, particle size and the packing properties on the one hand, and the degree of saturation and tensile stress on the other hand.

Then, the problem of mechanical resistance of agglomerates was approached by DEM simulations. First, simulations were performed on an assembly of particles subjected to capillary forces. The phenomenological model was used as a reference to validate the numerical simulation results. After validation, numerical simulations were used to study the mechanical behaviour of wet or dry cakes subjected to compression. These results constitute an important step in the description of the mechanisms activated by the relative humidity, which are at the origin of the caking of the powders. An extension to the powders in the presence of cohesive bonds in solid form was also proposed. The use of an Euler-Bernoulli beam to model the solid cohesive links and powerful numerical tools made it possible to characterize the mechanical behaviour of a powder compact. The comparison of experimental results obtained by brazilian and shear tests with the numerical predictions from DEM simulations showed a good overall match between experimental behaviour and simulations. These very encouraging results clearly demonstrate that the choice of a discrete approach is fully justified, on the one hand, by the intrinsic nature (granular character) of the powders, and on the other hand, by a modelling of the mechanisms of rupture at cohesive links.

Acknowledgements

Join support by Région Haut-de-France (CR Picardie) and EU funding (FEDER) for MOTTAMORPH project are gratefully acknowledged.

Nomenclature

a_w	Water activity
R	Particles radius
h	Interparticle gap
h^*	Dimensionless interparticle gap
V_L	Volume liquid
$\underline{T}$	Temperature
F_{cap}	Capillary force of a binary contact
S	Degree of saturation
ψ	Filling angle
$\varrho_{1,2}$	Principal radii of curvature
γ	Vapor-liquid surface tension
v_L	Molar volume of liquid
σ_T	Tensile strength
σ	Tensile stress
d_p	Particle diameter
d_m	Mean diameter
ε	Mean void fraction
$\ddot{u}_i, \ddot{\theta}_i$	Linear and angular acceleration of particle i
m_i, I_i	Mass and the moment of inertia of particle i
F_i^{ext}, M_i^{ext}	External force and moment vectors acting on particle i
$F^{j\to i}, M^{j\to i}$	Force and moment vectors due to the action of particle j on particle i
$k_{n,t}$	Normal/tangential contact stiffness
$c_{n,t}$	Normal/tangential damping coefficient
μ	Coulomb's friction coefficient
m^*	Reduced mass of two particles in contact
$\delta_{n,t}$	Normal/tangential relative displacement
$v_{n,t}$	Normal/tangential relative velocity
$c_{n,t}$	The normal and tangential damping coefficient
$F_{n,t}$	Normal, tangential contact force
Δt	Time step
E	Young's modulus of the particle
v	Poisson's ratio of the particle
R_{eff}	Effective radius
E_{eff}	Effective Young's modulus
G_{eff}	Effective shear modulus
E_M	Macroscopic Young's modulus of the caked powder
v_M	Macroscopic Poisson's ratio of the caked powder
E_μ	Young's modulus of the beam
G_μ	Shear modulus of the beam
A_μ	Cross section of the beam
a_μ	Radius of the cross section of the beam
L_μ	Length of the beam
r_μ	Dimensionless parameter
$u_{n,t,f}$	Degrees of freedom in translation of the beam
$\theta_{n,t,f}$	Degrees of freedom in rotation of the beam

$K_{n,t}$	Normal/tangential stiffness of the beam
S_n	Torsion stiffness of the beam
n, t, f	Subscripts related to the normal, tangential and bending effects
$d_{i,j}$	Intercenter vector connecting particles i and j
$f_{i,j}$	Cohesive force vector acting on the particles i and j
V_i	Volume of the particle i
Z_i	Coordination number of the particle i
$\bar{\sigma}_p^i$	Equivalent Cauchy stress tensor of the particle i

References

1. Charpentier, J.C. and T.F. McKenna, *Managing complex systems: some trends for the future of chemical and process engineering.* Chemical Engineering Science, 2004. **59**(8): p. 1617-1640.
2. Afrassiabian, Z., et al., *An overview of the role of capillary condensation in wet caking of powders.* Chemical Engineering Research and Design, 2016. **110**: p. 245-254.
3. Zafar, U., et al., *A review of bulk powder caking.* Powder Technology, 2017. **313**: p. 389-401.
4. Carpin, M., et al., *Caking of lactose: A critical review.* Trends in Food Science & Technology, 2016. **53**: p. 1-12.
5. Afrassiabian, Z., M. Guessasma, and K. Saleh, *A study on the caking behaviour of binary mixtures of lactose due to solid-state crystallisation of the amorphous phase.* Chemical Engineering Research and Design, 2019. **147**: p. 354-366.
6. Afrassiabian, Z., *Multiscale investigation of caking phenomenon of polymorphic powders: from physico-chemical aspects to industrial applications*. 2019, PhD thesis, Université de Technologie de Compiègne.
7. Samain, S., *Caractérisation multi-échelle de l'efflorescence et du mottage du saccharose*. 2017, Université de Technologie de Compiègne.
8. Rumpf, H., *The strength of granules and agglomerates*, in *Agglomeration*, W.A. Knepper, Editor. 1962, John Wiley: New York. p. 379-418.
9. Delenne, J.Y., et al., *Compressive strength of an unsaturated granular material during cementation.* Powder Technology, 2011. **208**(2): p. 308-311.
10. Kim, B.S., S.W. Park, and S. Kato, *DEM simulation of collapse behaviours of unsaturated granular materials under general stress states.* Computers and Geotechnics, 2012. **42**: p. 52-61.
11. Cundall, P.A. and O. Strack, *A discrete numerical model for granular assemblies.* Geotechnique, 1979. **29**: p. 47-65.
12. Golshan, S., R. Zarghami, and K. Saleh, *Modelling Methods for Gravity Flow of Granular Solids in Silos.* Reviews in Chemical Engineering, 2019.
13. Norourzi, H., et al., *Coupled CFD-DEM Modeling: Formulation, Implementation and Application to Multiphase Flows*. 2016.
14. Martin, S., et al., *Simulation of sintering using a Non Smooth Discrete Element Method. Application to the study of rearrangement.* Computational Materials Science, 2014. **84**: p. 31-39.
15. Leclerc, W., *Discrete element method to simulate the elastic behavior of 3D heterogeneous continuous media.* International Journal of Solids and Structures, 2017. **121**: p. 86-102.

16. André, D., et al., *Discrete element method to simulate continuous material by using the cohesive beam model.* Computer Methods in Applied Mechanics and Engineering, 2012. **213-216**: p. 113-125.
17. Haddad, H., M. Guessasma, and J. Fortin, *A DEM–FEM coupling based approach simulating thermomechanical behaviour of frictional bodies with interface layer.* International Journal of Solids and Structures, 2016. **81**: p. 203-218.
18. Leclerc, W., H. Haddad, and M. Guessasma, *On the suitability of a Discrete Element Method to simulate cracks initiation and propagation in heterogeneous media.* International Journal of Solids and Structures, 2017. **108**: p. 98-114.
19. Gagneux, G. and O. Millet, *Analytic Calculation of Capillary Bridge Properties Deduced as an Inverse Problem from Experimental Data.* Transport in Porous Media, 2014. **105**(1): p. 117-139.
20. Lubachevsky, B.D. and F.H. Stillinger, *Geometric properties of random disk packings.* Journal of Statistical Physics, 1990. **60**(5): p. 561-583.
21. Zhou, M., *A new look at the atomic level virial stress: on continuum-molecular system equivalence.* Proceedings of the Royal Society of London. Series A: Mathematical, Physical and Engineering Sciences, 2003. **459**(2037): p. 2347-2392.
22. Jebahi, M., et al., *Simulation of Vickers indentation of silica glass.* Journal of Non-Crystalline Solids, 2013. **378**: p. 15-24.
23. Samain, S., et al., *Characterization of caking for crystalline materials: comparison and statistical analysis of three mechanical tests.* Chemical Engineering Science, 2018.

Figure1. Schematic representation of a pendular liquid bridge between two equal-sized particles

Figure 2. Euler-Bernoulli beam type cohesion model [19]

Figure 3. Binary contacts for different separating distances (from left to right: $2h^*$=0.02; 0.08; 0.20 and 0.30)

Figure 4. (a) Evolution of the compactness of regular stacks: CS, CC and CFC, (b) Densified state of a CC stack

Figure 5. Evolution of a packing of 2000 particles: (a) Kinetic energy during the stabilization phase and the quasi-static tensile test; (b) Capillary bridges (S = 1.28%); (c) Equilibrium velocity field

Figure 6. Variation of the time-weighted tensile stress as a function of the relative elongation of the packing

Figure 7. (a) traction curve; (b) time evolution of the coordination number

Figure 8. (a) Comparison of the numerical and experimental compression curves; (b) tensile stress; (c) qualitative representation of the fracture during the Brazilian test

Figure 9. (a) Comparison of the numerical and experimental shear curves; (b) Qualitative representation of the rupture during the shear test

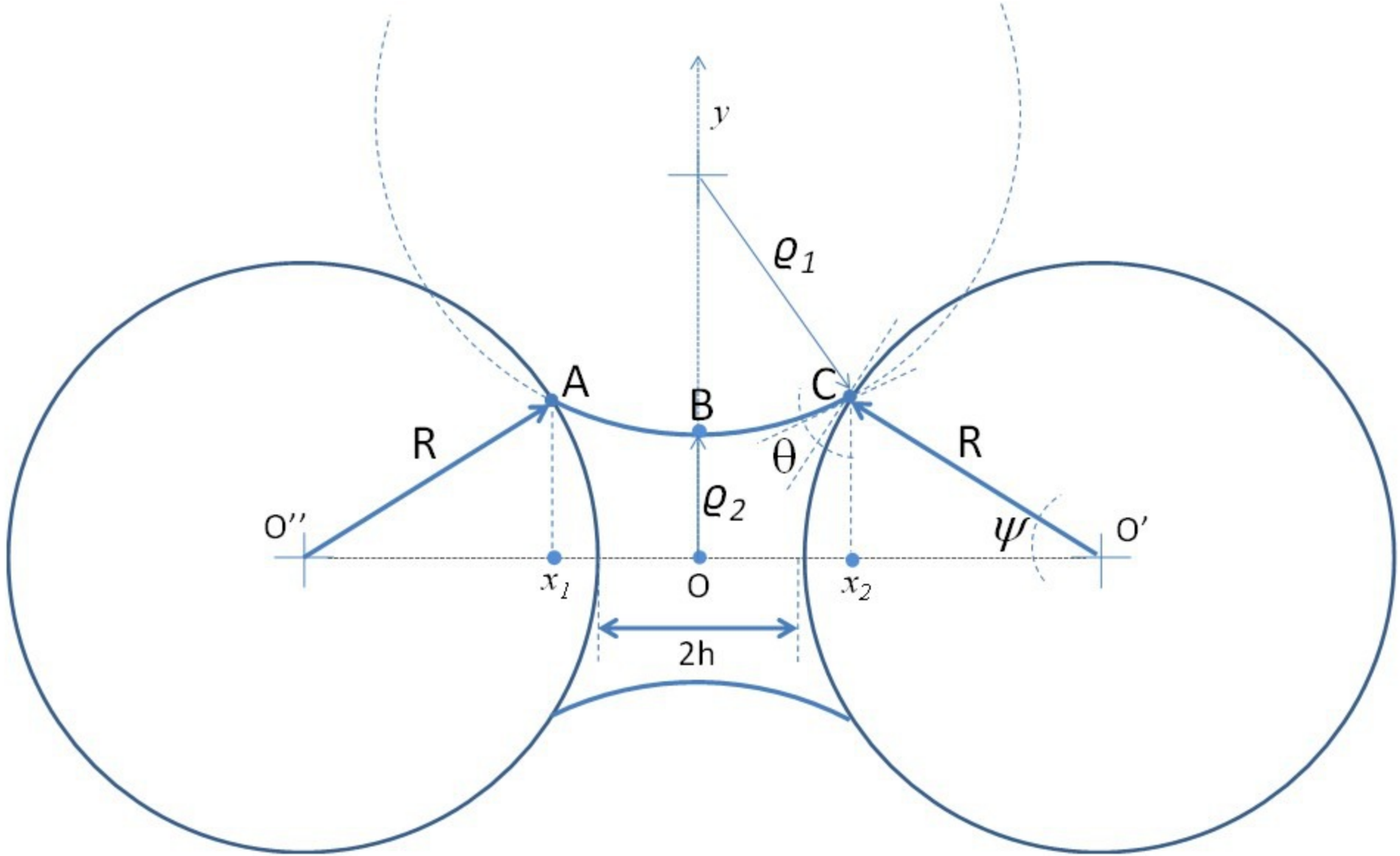

Figure1. Schematic representation of a pendular liquid bridge between two equal-sized particles

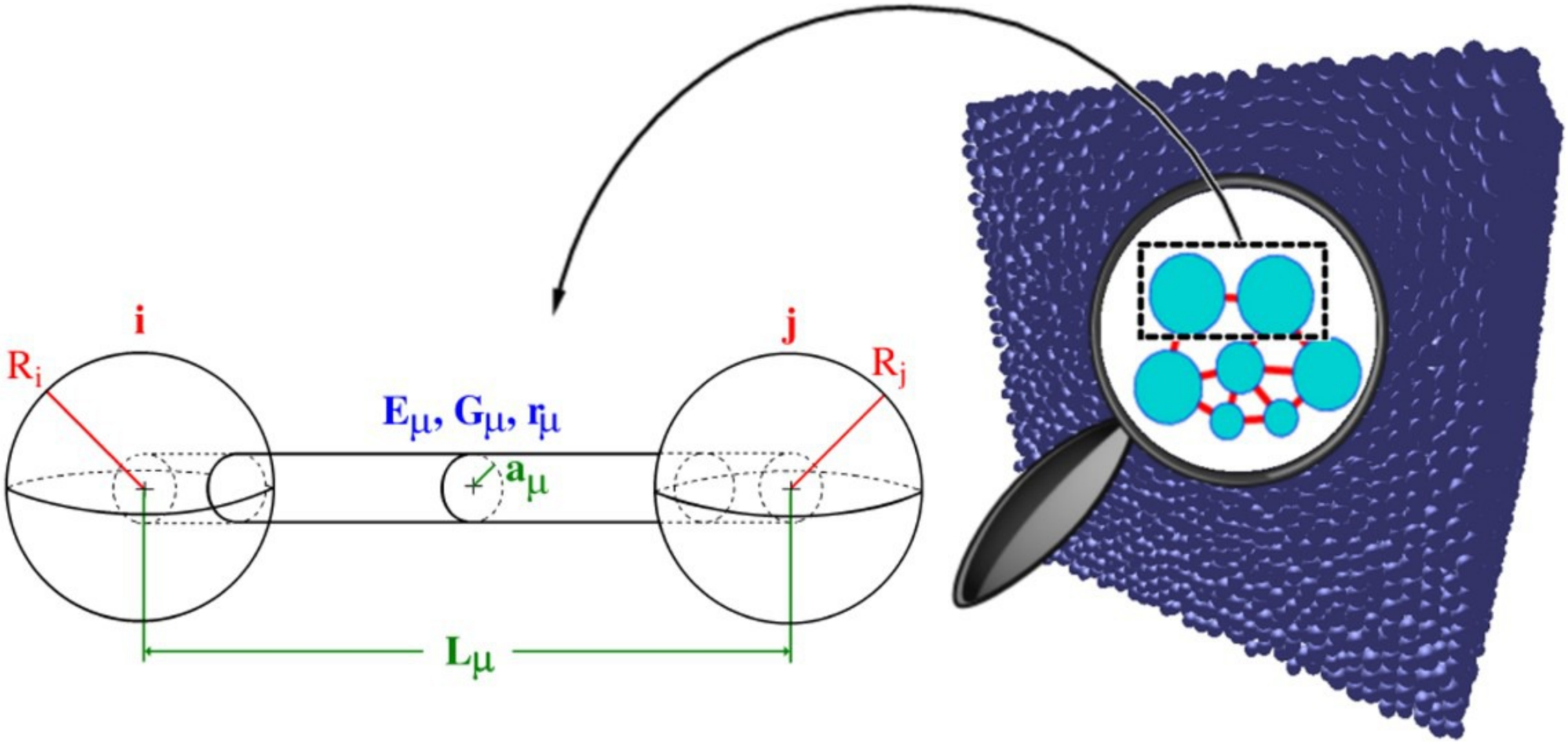

Figure 2. Euler-Bernoulli beam type cohesion model [19]

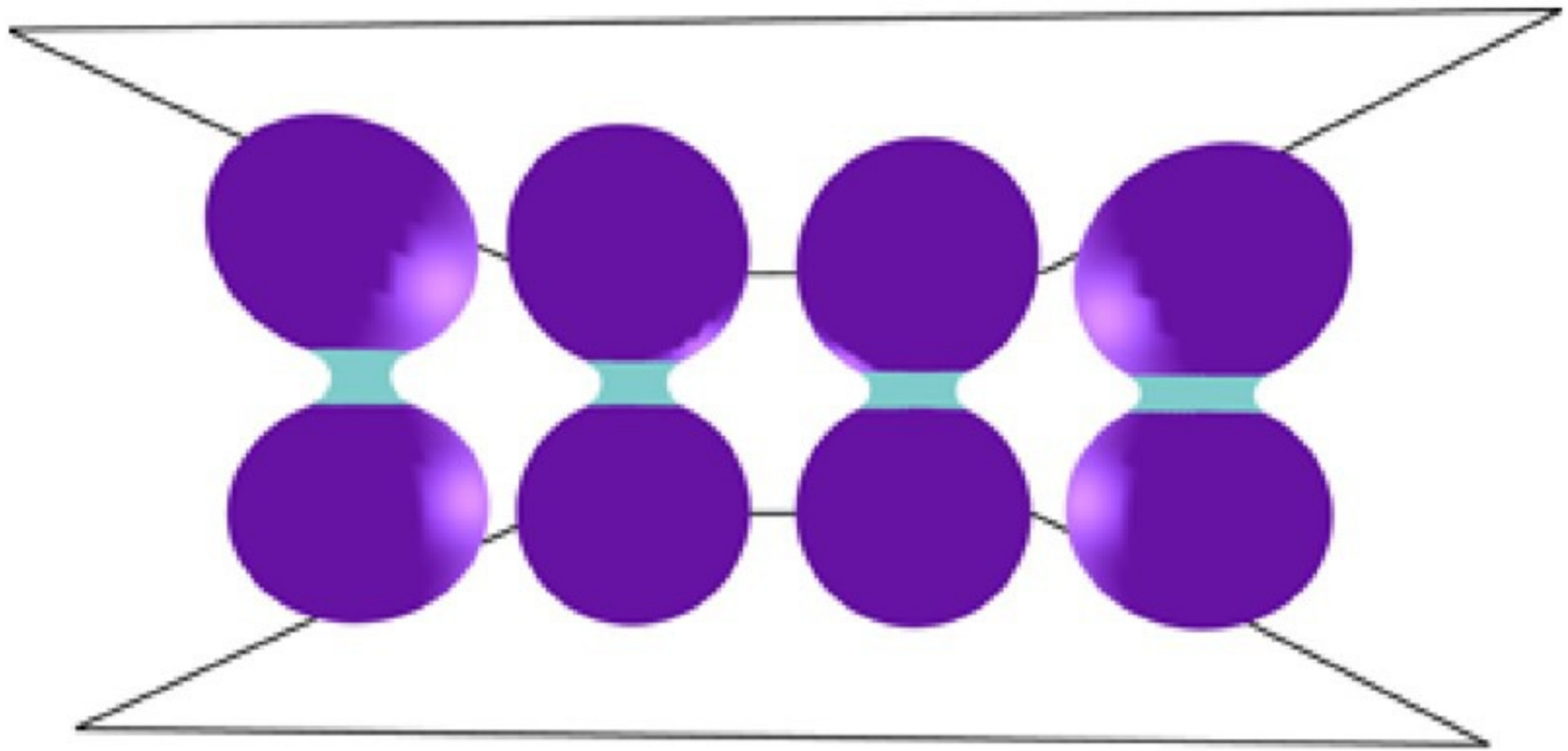

Figure 3. Binary contacts for different separating distances (from left to right: $2h^* = 0.02; 0.08; 0.20\ and\ 0.30$)

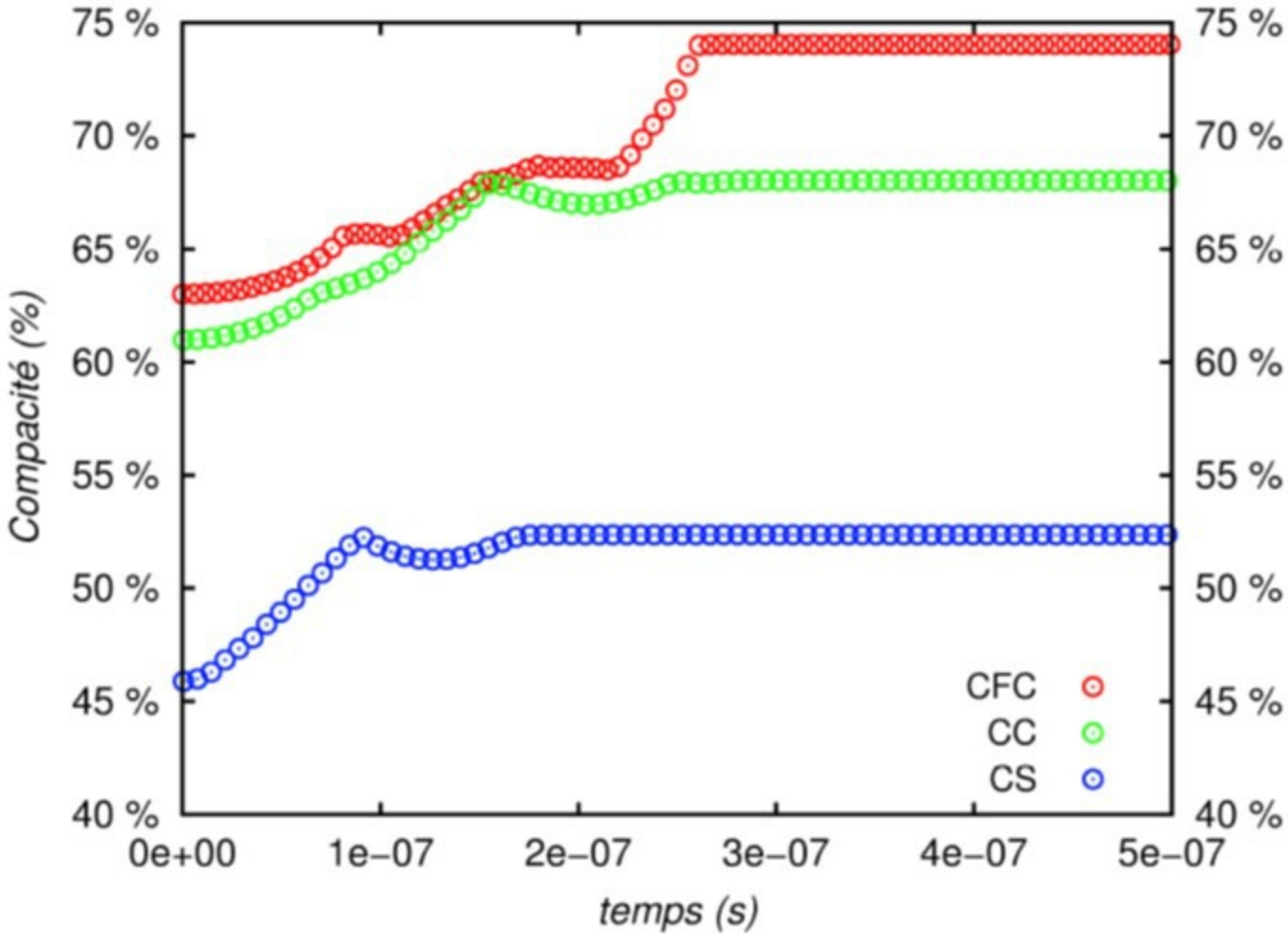

(a)

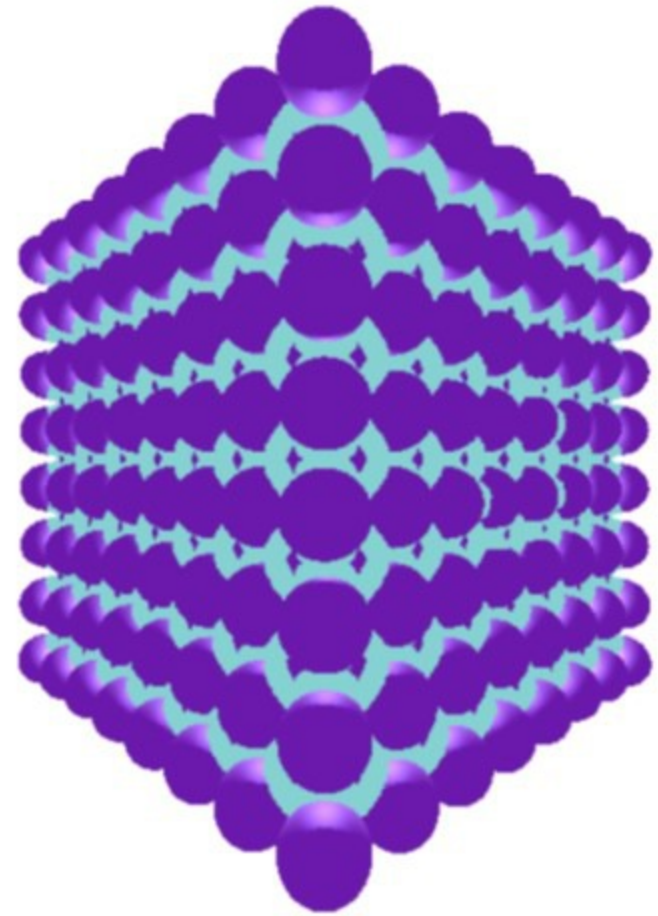

(b)

Figure 4. (a) Evolution of the compactness of regular stacks: CS, CC and CFC, (b) Densified state of a CC stack

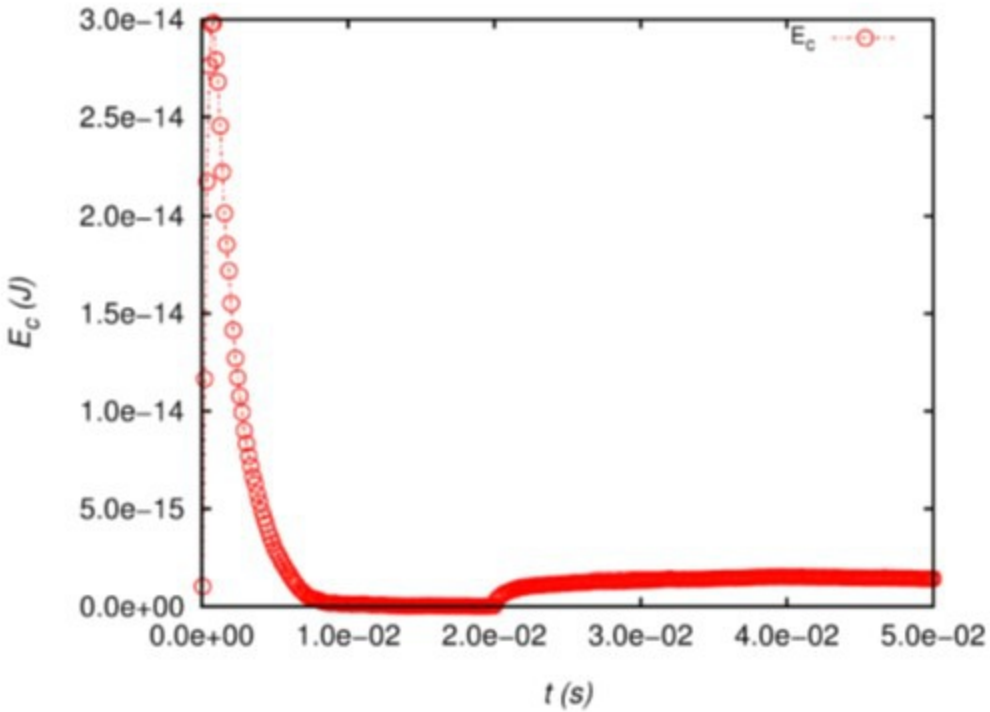

(a)

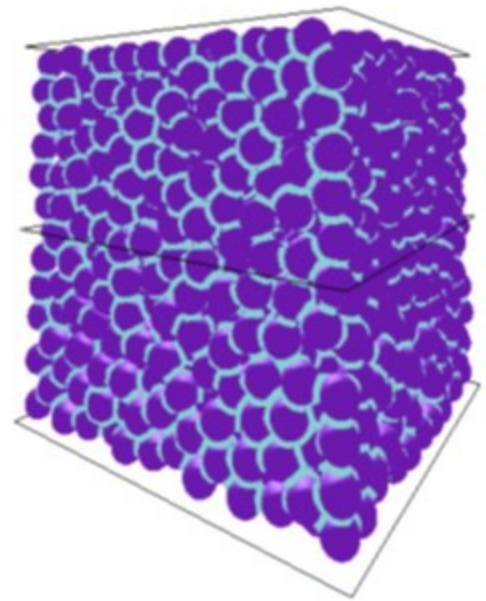

(b)

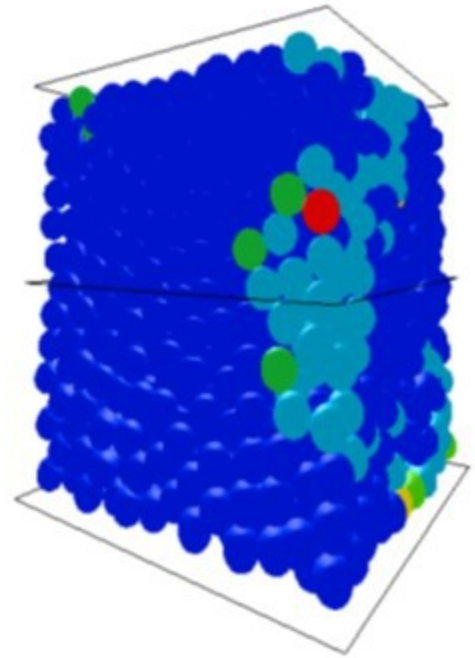

(c)

Figure 5. Evolution of a packing of 2000 particles: (a) Kinetic energy during the stabilization phase and the quasi-static tensile test; (b) Capillary bridges (S = 1.28%); (c) Equilibrium velocity field

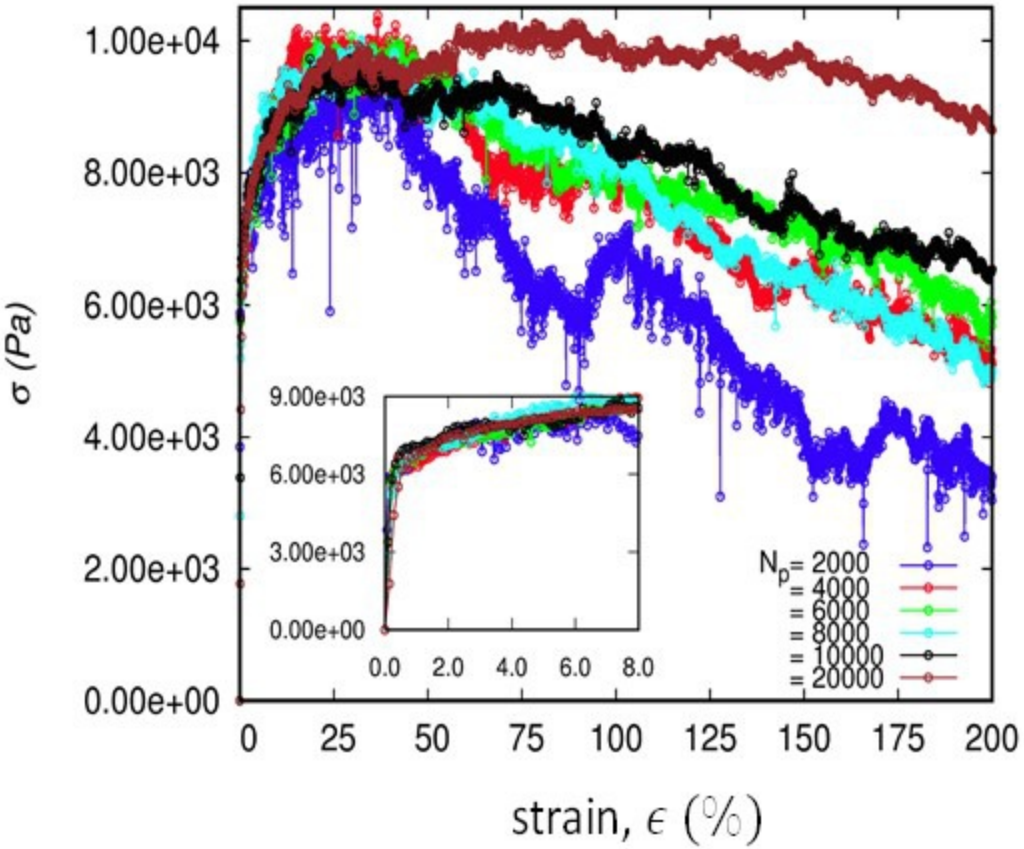

(a)

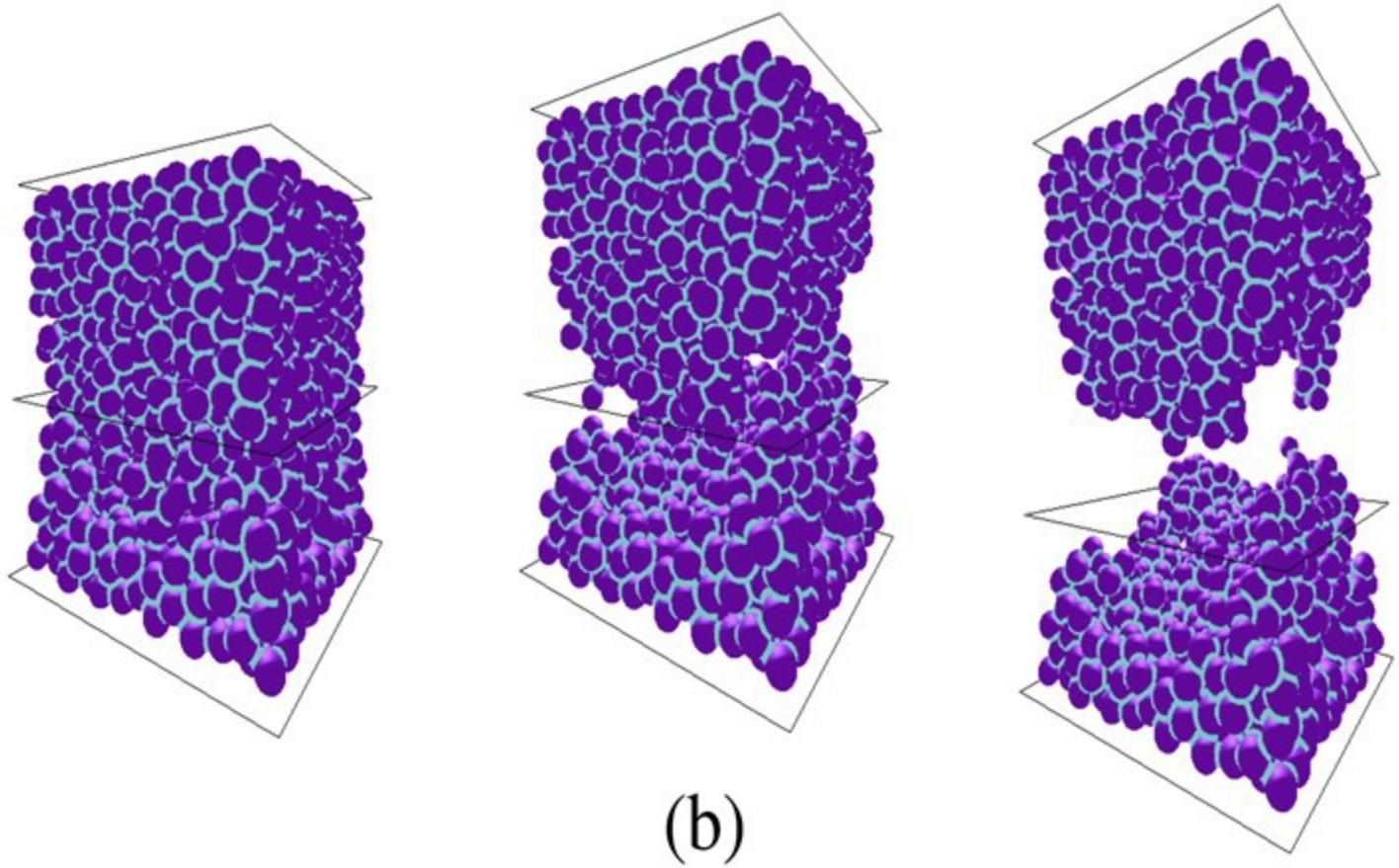

(b)

Figure 6. Variation of the time-weighted tensile stress as a function of the relative elongation of the packing

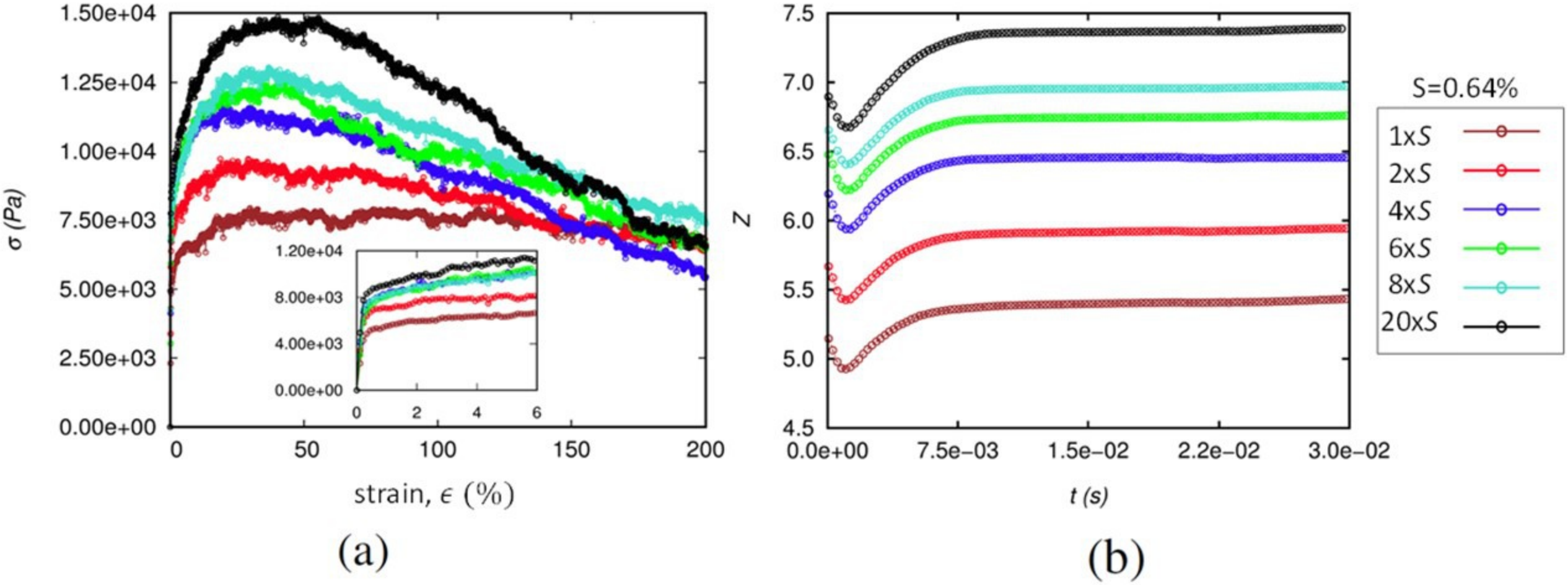

Figure 7. (a) traction curve; (b) time evolution of the coordination number

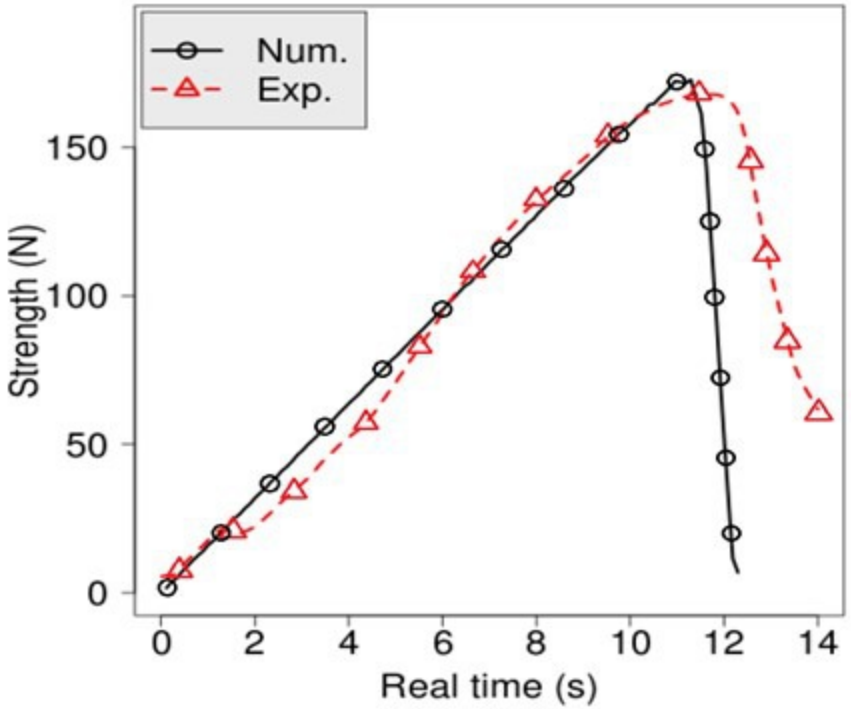

(a)

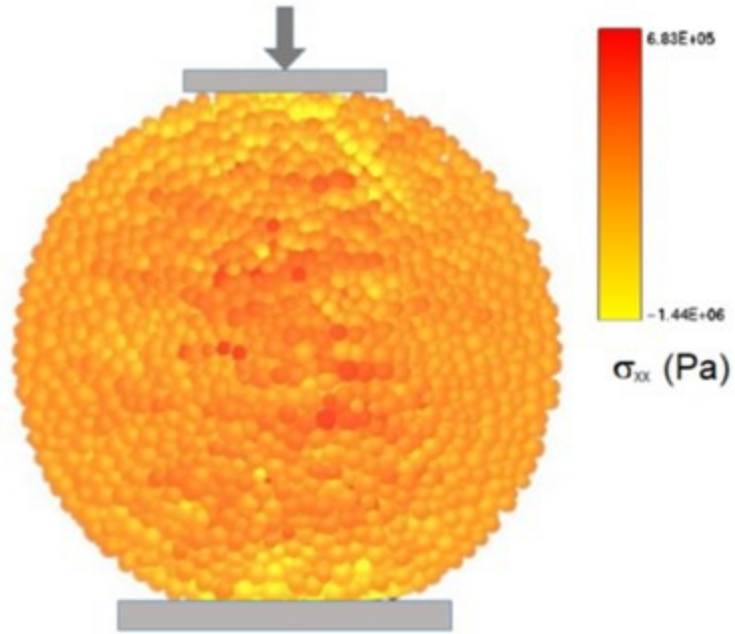

(b)

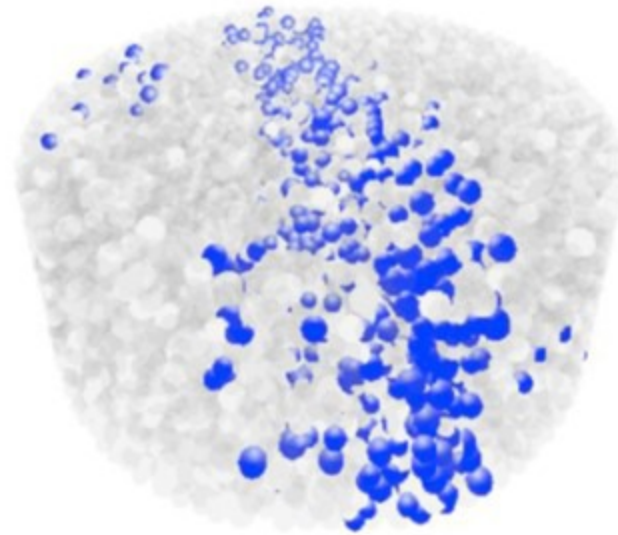

(c)

Figure 8. (a) Comparison of the numerical and experimental compression curves; (b) tensile stress; (c) qualitative representation of the fracture during the Brazilian test

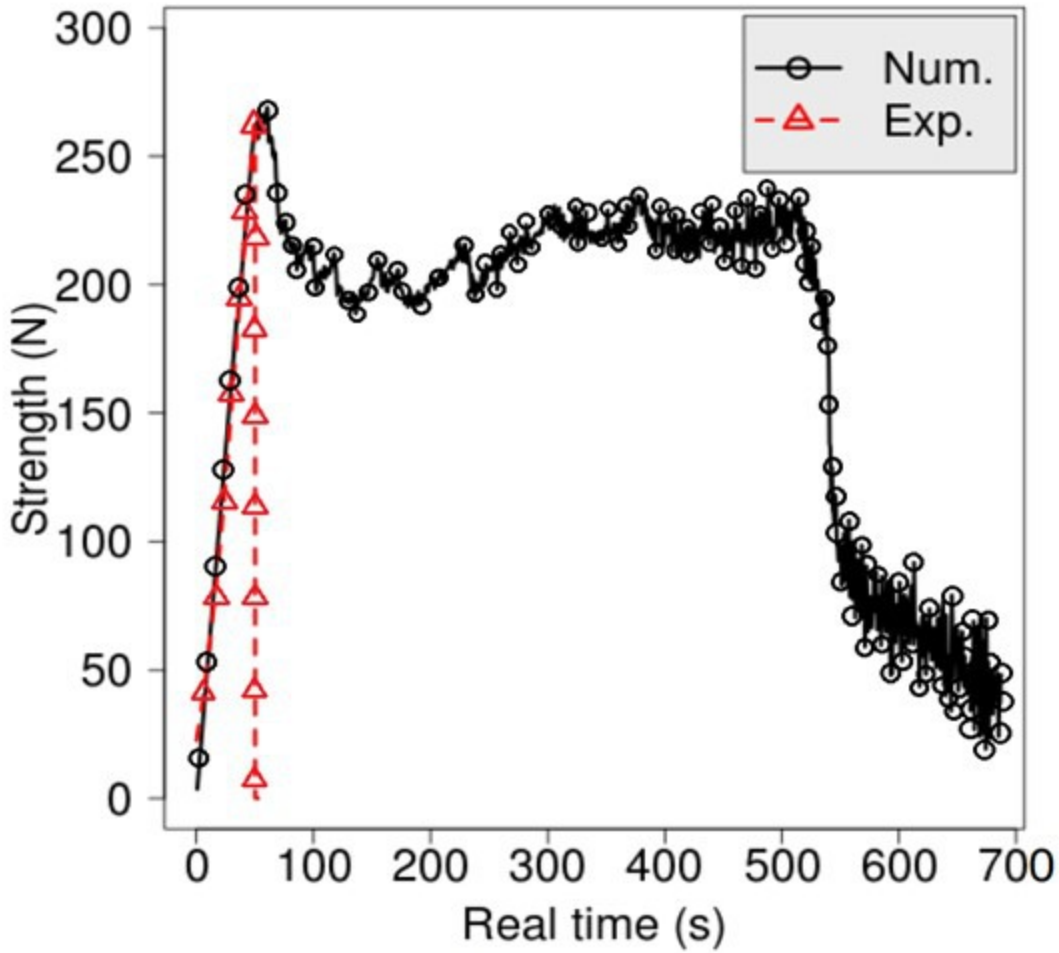

(a)

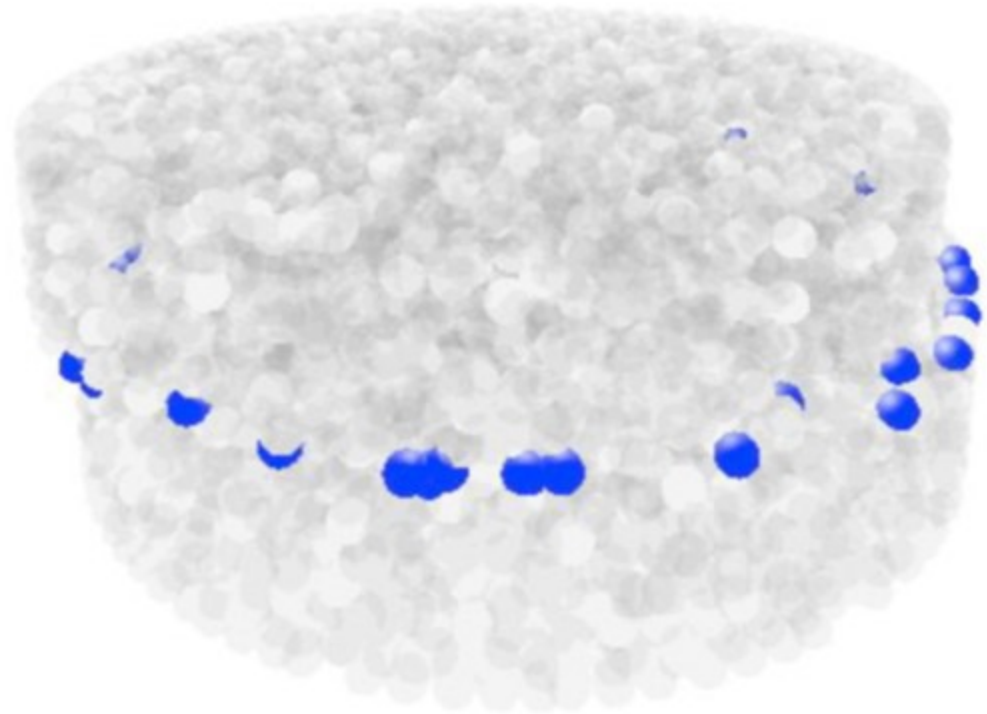

(b)

Figure 9. (a) Comparison of the numerical and experimental shear curves; (b) Qualitative representation of the rupture during the shear test

Table 1: Characteristics of the powder compacts for the tensile tests

Sample dimensions (m^3)	10^{-12}
Interval of the number of particles	$[2 \times 10^3 - \ 2 \times 10^4]$
Interval of the particle radius R (μm)	$[2 - 4]$
Density of particle material (kg/m^3)	1500
Interval of degree of saturation (%)	$[0.64 - 12.8]$
Mean void fraction φ	0.5
Velocity of the tensile test (m/s)	10^{-4}
Time step (s)	10^{-7}

Table 2: Characteristics of the caked powder for the Brazilian and shear tests

Sample diameter (mm)	40
Sample thickness (mm)	16
Mean diameter of particles d_m (μm)	675
Density of particle material (kg/m^3)	1515
Mean void fraction φ	0.64
Macroscopic Young's modulus of the sample E_M (GPa)	5.1
Macroscopic Poisson's ratio of the sample υ_M	0.24
Dimensionless radius r_μ	0.72
Young's modulus of the beam E_μ (GPa)	0.44
Strength limit of particle (MPa)	0.8
Velocity of the test (m/s)	$1{,}67\ 10^{-5}$
Time step (s)	$5.42\ 10^{-5}$

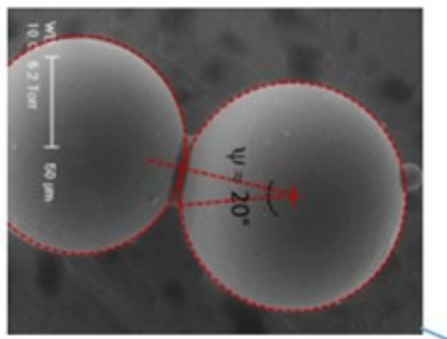

experimental

phenomenological model

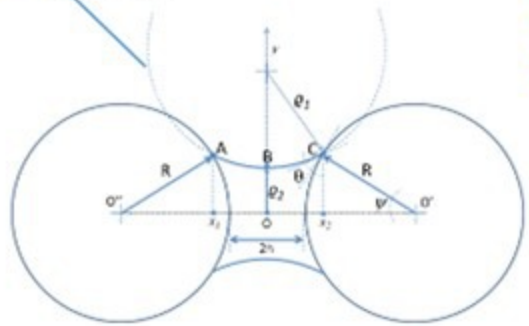

DEM + Capillary

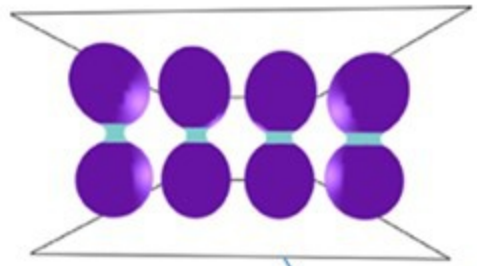

DEM wet assembly

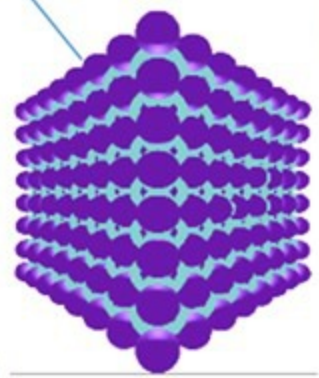

DEM solid bridge